Nigerian Journal of Applied Physics (NJAP)
ISSN Print: 3115-5871
ISSN Online: 3115-588X
DOI: https://doi.org/10.62292/njap-v2i2-2026-54
Volume 2(2), June 2026

Eco-Friendly Plant-Assisted Synthesis of Zinc Oxide Nanoparticles from *Mangifera indica* and *Carica papaya* Leaf Extracts: A Comprehensive Structural, Optical, and Electrical Study

***[1]Olanrewaju Oludotun Daramola, [2]Joshua Toyin Adeleke, [3]Adewale Bidemi Ayeni, [4]Lois Ayomide Adeleke and [1]Babatunde Abraham Idowu**

[1]Department of Physics, Lead City University, Ibadan, Oyo State, Nigeria.
[2] Physical Science Department, Osun State University, Oshogbo, Osun State, Nigeria.
[3]Department of Physics, Thomas Aderemi University, Oko, Kwara State, Nigeria.
[4]Department of Physics, Federal University of Agriculture and Development Studies, Iragbiji, Osun State, Nigeria.

[*]Corresponding author's email: daramola.olanrewaju@lcu.edu.ng Phone: +234-805-305-2676
ORCID: https://orcid.org/0000-0001-5548-4434

ABSTRACT
Green synthesis of zinc oxide (ZnO) nanoparticles (NPs) using plant extracts has attracted increasing attention due to its eco-friendly, cost-effective, and sustainable nature. In this study, ZnO nanoparticles were successfully synthesized using aqueous leaf extracts of *Mangifera indica* and *Carica papaya*, where plant phytochemicals acted as reducing and stabilizing agents, eliminating the need for toxic chemicals. Powder X-ray diffraction (XRD) analysis confirmed that the synthesized ZnO NPs crystallized in a cubic phase consistent with JCPDS card no. 36-1451. The average crystallite sizes were 17.25 nm for *Mangifera. Indica*-derived ZnO, and 33.27 nm for *Carica papaya*-derived ZnO, as estimated using the Scherrer equation. UV–Vis spectroscopy showed characteristic absorption peaks at 299 nm and 303 nm, respectively, with variations in direct and indirect band gaps attributed to particle size differences and minor carbon impurities (2.0–3.2%). SEM analysis revealed predominantly spherical and flower-like morphologies with uniform distribution, while EDX confirmed Zn and O as the major elemental constituents. Electrical conductivity measurements indicated higher conductivity for *Mangifera indica*-derived ZnO (24.96 mS) compared to *Carica papaya*-derived ZnO (16.24 mS), suggesting superior dielectric potential. Overall, the study demonstrates that green synthesis using plant extracts is an effective route for producing ZnO nanoparticles suitable for applications in electronics, optoelectronics, photocatalysis, cosmetics, and biomedical fields.

Keywords:
Green synthesis,
Zinc oxide nanoparticles,
Mangifera indica,
Carica papaya,
Optoelectronic applications.

INTRODUCTION
Nanotechnology is an emerging field with the potential to revolutionize several scientific and technological disciplines due to the unique size-dependent properties of nanomaterials. Nanoparticles, typically ranging from 1–100 nm, possess a high surface area-to-volume ratio, resulting in enhanced thermal conductivity, chemical stability, nonlinear optical behavior, and catalytic activity compared to their bulk counterparts (Fakhari *et al*., 2019; Agarwal *et al*., 2017). In recent years, the integration of nanotechnology with green chemistry principles has gained significant attention. Green chemistry primarily addresses two key challenges: the safe management of hazardous industrial waste and the development of sustainable synthetic routes that eliminate or minimize the use of toxic substances (Gul *et al*., 2021). This approach emphasizes environmentally benign raw materials, safer processing methods, and reduced ecological impact while promoting responsibility among scientists and manufacturers (Viana *et al.*, 2020; Ansari *et al.*, 2020).
Plant-mediated green synthesis of nanoparticles has emerged as a promising alternative to conventional chemical and physical methods, which are often energy-intensive and environmentally harmful. Plant extracts serve as effective reducing and capping agents due to their rich phytochemical content, enabling safe and cost-effective nanoparticle production. Zinc oxide (ZnO) nanoparticles, in particular, are attractive for sustainable

and renewable energy applications owing to their abundance, chemical stability, low cost, and ease of processing. Their structural and surface properties significantly influence performance in energy harvesting, conversion, and storage systems, contributing to environmentally friendly solutions for global energy challenges (Wahid *et al*., 2020).

Despite considerable progress in the plant mediated green synthesis of ZnO nanoparticles, most existing studies examine the structural, optical, or morphological behaviour of a single plant-derived ZnO system in isolation, with comparatively few studies subjecting two botanically distinct extracts to identical synthesis, deposition, and characterization conditions for direct comparison. In addition, structural and optical characterization of green-synthesized ZnO nanoparticles is well documented in the literature, but this is rarely coupled with electrical conductivity measurements of the corresponding ZnO thin films deposited on conductive substrates such as Indium Tin Oxide (ITO), information that is essential for evaluating their suitability for optoelectronic, sensing, and energy-related device applications. This gap limits the extent to which clear structure property performance relationships can be established to guide the selection of plant extracts for specific technological uses. The present study addresses this gap by providing a comprehensive, side by side structural, optical, and electrical investigation of ZnO nanoparticles synthesized from *Mangifera indica* and *Carica papaya* leaf extracts, deposited on ITO substrates and processed under identical conditions, thereby linking their structural and optical properties directly to electrical performance.

This study focuses on the green synthesis of ZnO nanoparticles using *Mangifera indica* (mango) and *Carica papaya* (pawpaw) leaf extracts as reducing and stabilizing agents. The synthesized nanoparticles were comparatively characterized using X-ray diffraction (XRD), UV–Visible spectroscopy, scanning electron microscopy with energy-dispersive spectroscopy (SEM/EDS), and electrical conductivity measurements. The findings provide evidence-based insights into the effectiveness of these plant extracts in nanoparticle formation and functional enhancement, contributing valuable knowledge to green nanotechnology research.

MATERIALS AND METHODS

Collecting the Plant Samples

Carica papaya and *Mangifera indica* leaves that appeared fresh and healthy were gathered from the Oremeji Area of Ibadan, Oyo State, Nigeria. The plants were recognized and verified. After four to five weeks of air drying in the shade, these samples were ground into a powder for subsequent use. Until they were needed, the powdered leaves were kept at room temperature in airtight containers.

Carica Papaya and *Mangifera Indica* Leaf Extract Preparation

As shown in figure 1, fifty grams of ground or powdered leaf samples of *Carica Papaya* and *Mangifera Indica* were combined with 600 ml of distilled water in 1000 ml beakers. After that, the beakers were covered with aluminum foil and left for a whole day. After settling, the liquid supernatant was sieved using a muslin bag and filtered out using filter paper with the smallest pore size. The filtrate was then put into centrifuge bottles with labels, as shown in the picture below. After centrifuging the filtrates for ten minutes at 1000 rpm, the supernatant was placed into sample bottle with clear labels.

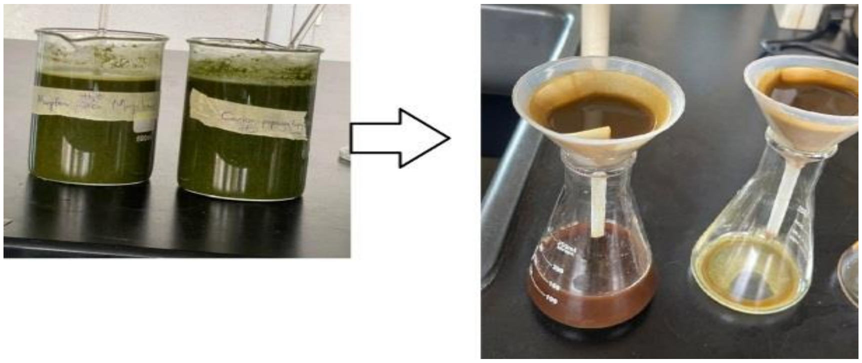

Figure 1: The cold water extraction process of *carica papaya* and *mangifera indica* leaf extract

Zinc nitrate ($Zn(NO_3)_2$), EMPLURA grade) served as the precursor for ZnO nanoparticle production. To create a 0.4 M solution, dissolve 7.574 g of $Zn(NO_3)_2$ in 100 mL of distilled water. Stir intermittently for 20 minutes until completely dissolved. The solution was divided equally into two conical flasks and magnetically swirled for 20 min. *Carica papaya* and *Mangifera indica* leaf extracts were then mixed individually in a 1:5 ratio (extract to precursor). Continuously stirred until colour changes and the pH was adjusted to neutral (pH 7; being mindful of application in biological interest the particle yield was low; having known that at pH between 8-9 it yield better) by gradually adding 0.4 M NaOH. The mixtures were agitated for 1 hour and 30 minutes, resulting in a sol-gel transition and a modest color change. The products were filtered, oven-dried at 60°C, and then annealed at 400°C for 2 hours to yield ZnO nanoparticles. The synthesis process was represented in figure 2:

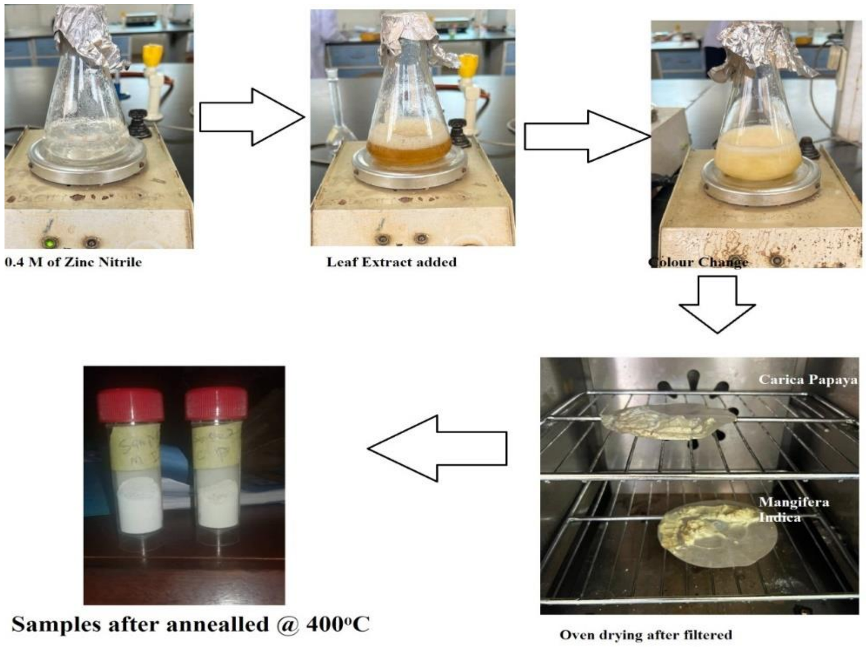

Figure 2: Synthesis process of Zinc Oxide Nanoparticle

Deposition of Zinc Oxide Nanopaticle on Indium doped Tin Oxide substrate

The solution obtained during nanoparticle synthesis was used to implant ZnO NPs on an Indium Tin Oxide (ITO) substrate. ITO panels measuring 2 cm by 4 cm were cut out using a diamond cutter and labeled for each sample of ZnO Nps from both leaf extracts. The ITO slides were first cleaned by rinsing them in distilled water and then washing them in methanol to remove grease. The spraying pyrolysis machine was set at a substrate temperature of 150ºC for all samples with a deposition period of 312 seconds (5 minutes and 12 seconds). For all samples, the nozzle height and distance to the substrate are both 20 cm, and the nozzle-to-substrate inclination slope distance is given by:

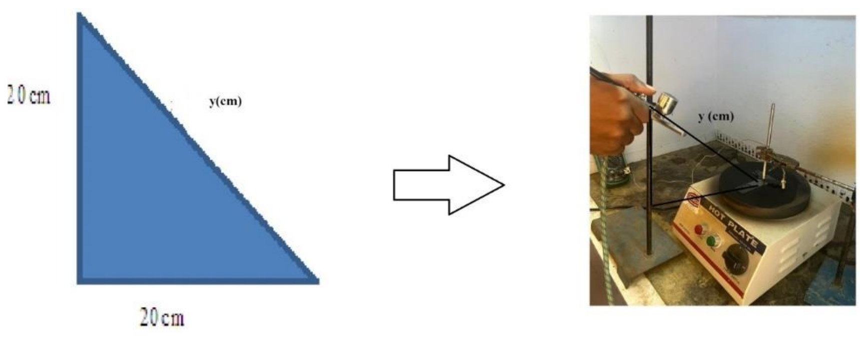

Figure 3: Spraying pyrolysis process showing nozzle-substrate distance

$$Nozzle - substrate\ distance\ y\ (cm) = \sqrt{height\ of\ the\ nozzle^2 + substrate\ horizontal\ distance^2}$$

$$y = \sqrt{20^2 + 20^2}$$

$$y = \sqrt{800cm^2} = 28.28\ cm$$

This was necessary because the nanoparticle yield was small for X-ray diffraction analysis. During the spraying process with the spray pyrolysis machine, pressure pumps and atomizers were also utilized. Figure 3 depicts the deposition process. The samples were then annealed for two hours at 350°C; this temperature was chosen to avoid denaturing the ITO conductivity.

RESULTS AND DISCUSSION

The samples were analyzed structurally using an X-ray diffractometer (XRD), morphologically with a scanning electron microscope (SEM/EDX), optically with UV-visible spectroscopy, and electrically with a digital conductivity tester. This section provided details on sample characteristics.

XRD (Structural)

Samples 1 and 2 were structurally characterized by powdered X-ray diffractometry (PXRD), with zinc oxide from Carica papaya and Mangifera indica nanoparticles, respectively. Their grain size was calculated using Equation 3.1, and the results were compared to conventional references. Equation 3.2 represents the lattice's d-space.

$$g = \frac{k\lambda}{\beta Cos\theta} \quad (1)$$

$$d_{space} = \frac{n\lambda}{2Sin\theta} \quad (2)$$

Where g is the grain size, K is a constant of value 0.94, λ is the wavelength of the XRD machine of value 0.15406 nm, β is the FWHM in degrees (but converted to radians) of the spectrum, d_{space} and Bragg's angle θ are obtained at 2θ that matches peaks in degrees, and n = 1.

Figure 4 shows the X-ray diffraction (XRD) patterns of green-synthesized ZnO nanoparticles placed on ITO substrates with extracts of *Mangifera indica* (Sample 1) and *Carica papaya* (Sample 2). The diffraction peaks at 2θ ≈ 31.7°, 34.4°, 36.2°, 47.5°, 56.6°, 62.8°, and 67.9° correspond to the hexagonal wurtzite ZnO crystallographic planes (100), (002), (101), (102), (110), (103), and (112). These peaks are consistent with the standard JCPDS card No. 36-1451, indicating the successful production of crystalline ZnO nanoparticles.

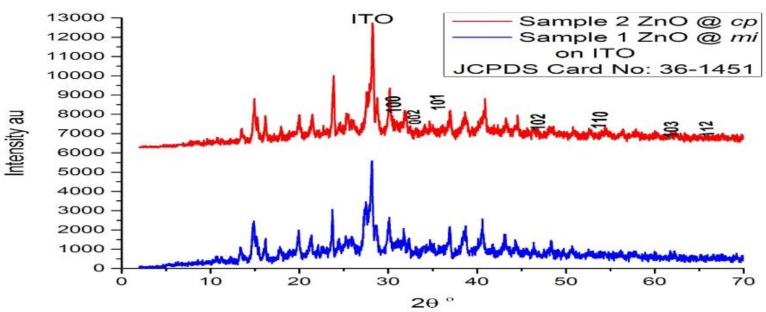

Figure 4: XRD for Zinc Oxide synthesized using *m. indica* and *c.papaya* leaf extracts tagged samples 1 and 2

Table 1: The grain size of the zinc oxide synthesized with leaf extract from *m. indica* and *c. papaya* leaf extracts for sample 1 and 2

Sample	2θ°	FWHM (β)°	Grain Size nm	Average grain size nm
1	32.00	2.03	4.26	
	47.50	0.30	30.24	17.25
2	31.82	0.37	23.34	
	47.50	0.21	43.20	33.27

UV-Visible (Optical)

The ZnO NPs samples and the extract of *M. indica* and *C. papaya* leaves are shown in Figure 5, UV-visible spectra. In the UV-visible spectrum, the nanoparticle samples have maxima at roughly 299 and 303 nm, respectively. However, ZnO suggests a considerable reduction in the signal strength at about 360 nm in the UV-visible spectrum of the ZnO NPs investigation Gur *et al.*, 2022. The Zinc oxide shows the absorption at 380 nm and pure nanoparticle is observed at 374 nm. The green ZnO Nps were found to have Eg values of 3.44 eV. Similarly, ZnO nanoparticles that were chemically produced showed a band gap energy of 3.35 eV (at the 370 nm absorption band) to indicate variations in their sizes. Due to the fact that particle size affects surface plasmon resonance (SPR), it should be noted that the two types of Nps displayed distinct absorption bands. The absorption band in the quantum confinement range moves towards a lower wavelength when the particle size decreases due to a rise in particle band gap energy. Consequently, our results demonstrate that the produced ZnO Nps have greater band gap energy than the chemically manufactured ZnO NPs, indicating their smaller size. It's possible that their significantly reduced size is due to these leaves extracts' powerful capping and lowering capabilities[4]. Hence, the band gaps for indirect were 3.61 and 3.56 eV for samples 1 and 2, respectively, while for the direct band gap, which is ZnO, it was revealed as 3.88 and 3.84 eV for samples 1 and 2, respectively.

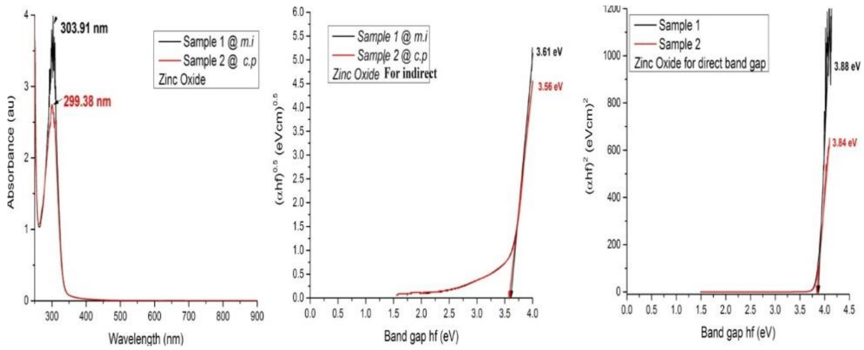

Figure 5: (a) The absorption spectrum of Zinc oxide (b) The indirect band gap using Tauc's equation (c) The direct band gap using tauc's equation for both synthesized through *mangifera indica* and *carica papaya* respectively

SEM/EDX (Morphology)

Scan Electron Microscopy (SEM) examinations were used to determine the size, shape, and structure of the synthesized ZnO NPs as shown in Figures 6. ZnO NPs micrographs demonstrated their homogeneous distribution, spherical shape, and nanoscale range. The SEM results showed that the size and form of the nanoparticles were altered while utilizing various leaves extracts.

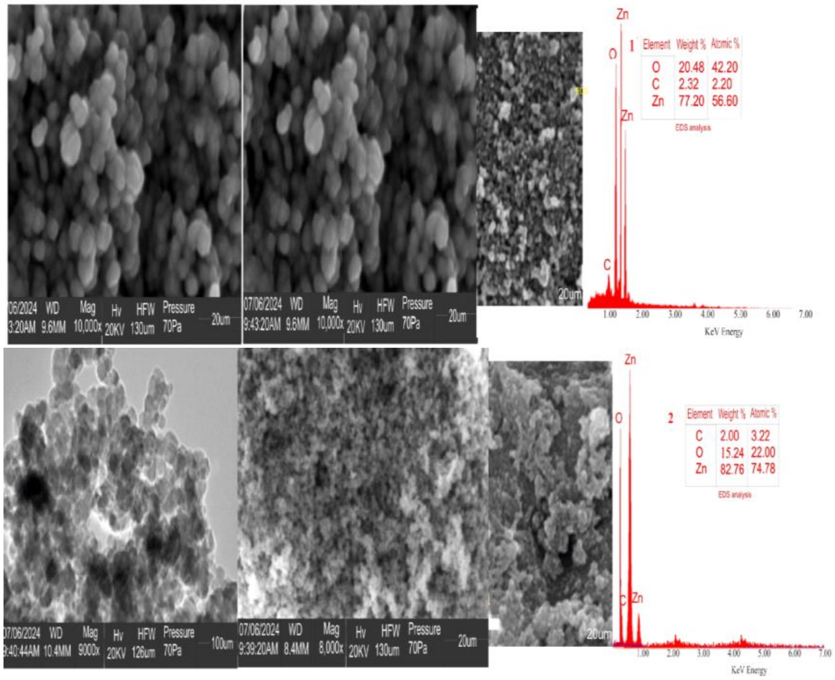

Figure 6: The SEM micrograph and EDS for samples 1 and 2; Zinc Oxide with *mangifera indica* and *carica papaya* respectively (Daramola *et al.*, 2025)

The produced ZnO NPs were analyzed by SEM and EDX for the morphological and elemental examination. ZnO NP production was verified by the EDX, which displayed a high signal in the oxygen and zinc areas. Furthermore, the *mangifera indica* ZnO NPs had a composition of 77.20% zinc, 20.48% oxygen, and 2.32% carbon and were hexagonal with aggregations. Their *carica papaya* counterparts, on the other hand, were spherical and comprised of 15.24% oxygen, 82.76% zinc, and 2.00% carbon. Also, EDX shows the dispersion of Zn in the range of 1.3 to 1.5 KeV, oxygen at 1.5 KeV, and carbon at 1.0 KeV for; *mangifera indica* leaf extract (Sample 1), while the EDX result shows the dispersion of Zn in the range of 0.5 to 1.0 KeV, oxygen, and carbon at 0.2 KeV for *carica papaya* leaf extract, as shown in figure 6.

Conductivity at the room temperature

The conductivity of the samples 1 and 2 in solution (the solution used for spray pyrolysis deposition) was determined using ECscan40 digital conductivity tester. The sample 1 Zinc oxide from the extract of *mangifera indica* shows higher conductivity of 24.96 mS while the sample 2 from *carica papaya* shows conductivity of 16.24 mS; all at the room temperature of 31.2 ^{o}C.

FTIR Data Analysis

The FT-IR spectra of the synthesized ZnO nanoparticles in Figure 7 were recorded in the range of 400–4000 cm^{-1} to identify the functional groups and confirm the formation of the ZnO phase. The transmittance profile exhibited multiple characteristic absorption bands, which were assigned with reference to recent literature. The broad absorption features observed in the range 3444–3456 cm^{-1} in Sample 1 (mi) and the corresponding 3444 cm^{-1} region in Sample 2 (cp) were attributed to O–H stretching vibrations of surface-adsorbed moisture and hydroxyl groups on the ZnO nanoparticle surface. These vibrations commonly occur due to hydrogen-bonded –OH groups, which may result from atmospheric water adsorption or remnants from synthesis solvents, consistent with previous reports of ZnO FT-IR spectra in the 3400–3600 cm^{-1} range Adeyemi *et al.*, (2025). The absorption modes at 2850 cm^{-1} and 2762 cm^{-1} can be ascribed to C–H stretching vibrations of residual organic moieties, potentially arising from capping agents or synthesis precursors. Such hydrocarbon-related bands were also identified in surface-modified ZnO composites, suggesting the presence of adsorbed organic species Singh *et al*., (2025). In the mid-infrared region, peaks at 2341, 2094, and 2357 cm^{-1} are indicative of adsorbed CO_2 or atmospheric contamination, or bending modes involving surface-bound functional groups. Similar features have been documented in ZnO nanoparticle FT-IR spectra and are often ascribed to physisorbed CO_2 or weakly bound species on nanoparticle surfaces El-Batal *et al*., (2025). A prominent absorption near 1616-1631 cm^{-1} can be assigned to H-O-H bending vibrations of water molecules, confirming adsorbed moisture within the sample matrix. Bands in this region have been similarly reported and are associated with the bending mode of physically adsorbed water on metal oxide surface Adeyemi *et al.*, (2025). In the fingerprint region, several distinct peaks between 800–1000 cm^{-1} (e.g., at 937, 813 cm^{-1}) are observed, which are attributable to various bending and stretching modes related to Zn-O lattice vibrations and residual related functional groups. These lower-energy features often correlate with surface defects or lattice dynamics in nanostructured ZnO Zhang *et al.*, (2024). The most characteristic absorption band confirming the formation of ZnO appears in the range 420–725 cm^{-1}, where strong peaks at 420.50 and 725.26 cm^{-1} were detected. Bands below 800 cm^{-1} are widely recognized as Zn–O stretching vibrations associated with the wurtzite ZnO lattice, which affirm successful nanoparticle synthesis. Reports in recent literature consistently assign strong bands in the 400–600 cm^{-1} regions to Zn–O phonon modes, validating our spectral observations Abdullahi *et al.*, (2024). Overall, the FT-IR spectrum confirms the presence of Zn–O bonds as the dominant structural feature of the nanoparticles, alongside adsorbed hydroxyl groups, atmospheric CO_2 species, and minor organic residues. The similarities between the two samples (mi and cp) suggest comparable surface chemistry and phase composition, with slight variations in the intensities of O–H and organic-associated bands indicating differences in surface adsorption or synthesis conditions Khan *et al.*, (2022) and Rana *et al.*, (2021).

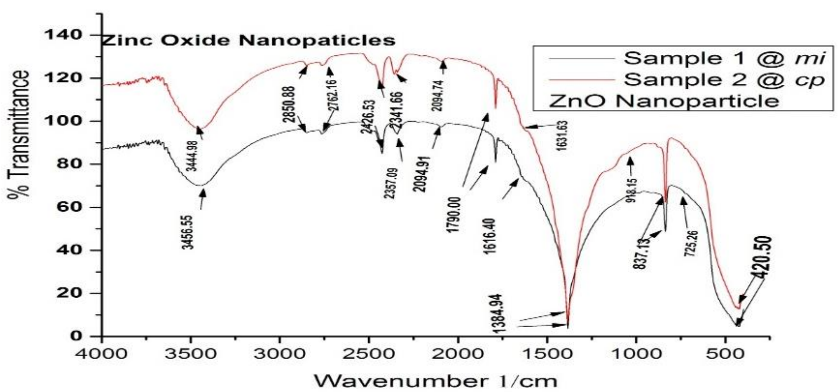

Figure 7: Fourier Transform Infrared Spectrum compared the Zinc oxide by the two different leaf extracts (Daramola *et al.*, 2025)

XRD Discussion

The 2θ peak values match the JCPDS card number 36-1451 as shown in Figure 4, confirming that the synthesized ZnO nanoparticles crystallize in the hexagonal wurtzite phase (space group $P6_3mc$), consistent with the diffraction planes indexed in Section 3.1. In this structure, each Zn^{2+} ion is tetrahedrally coordinated to four O^{2-} ions, and each O^{2-} ion is likewise coordinated to four Zn^{2+} ions, giving alternating close-packed layers of Zn and O ions stacked along the c-axis. This tetrahedral coordination is characteristic of the wurtzite lattice and accounts for the non-centrosymmetric, polar structure responsible for the piezoelectric and pyroelectric behaviour commonly reported for ZnO nanomaterials. The selected peak was used to determine the grain sizes using the Scherrer equation (Equation 3.1); the average grain size for zinc oxide synthesized using *mangifera indica* shows a grain size of 17.25 nm against the 33.27 nm shown by *Carica papaya*. The grain sizes of the two extracts fall within the nanoparticle range of 1-100 nm and are comparable to the 18-45 nm range reported for other green-synthesized ZnO nanoparticles, which likewise confirmed a hexagonal (wurtzite) morphology, as illustrated in Figure 8, Fakhari *et al.,* (2019); Elumalai, K., & Velmurugan (2015) and Singh *et al.,* (2019)

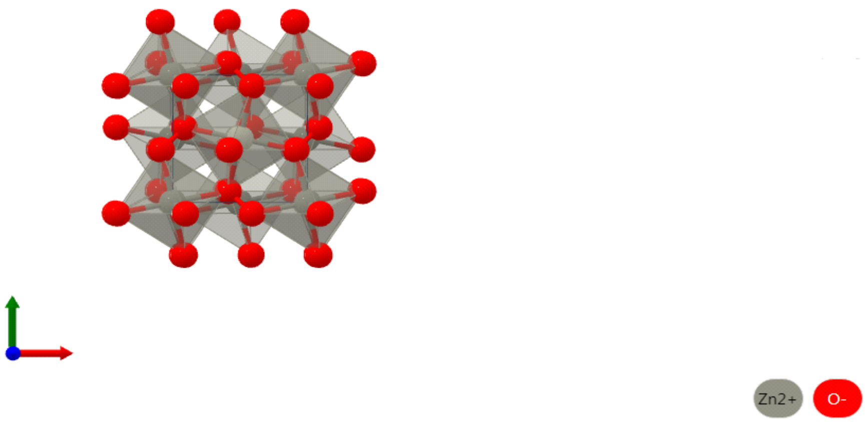

Figure 8: The cubic crystal structure for Zinc oxide (wurtzite) with XRD spectral closely matched generated by material explorer (Material explorer; https://next-gen.materialsproject.org/materials

Optical Characterization Discussion

The UV-Vis plot (left) shows strong absorbance in the UV region, with prominent peaks around 299-304 nm for both samples (m.i and c.p), indicating that ZnO strongly absorbs high energy (short wavelength) UV photons. This is typical for wide band gap semiconductors.

Real ZnO materials typically show a UV absorption edge around 360-380 nm, corresponding to electronic transitions from the valence to conduction band. For example, studies report a UV absorption peak/edge near 368–380 nm for ZnO nanostructures and thin films in UV-Vis spectra, consistent with band-edge absorption behavior in high-quality ZnO.

Interpretation: Peaks near 300 nm suggest significant absorption in the near UV region. Slight differences in peak positions between samples may arise from variations in particle size, defect states, or synthesis method, which affect electronic states and absorption intensity. Extrapolating the linear regions to the photon energy axis yields band gap energies around: 3.61 eV for Sample 1 (m.i) and 3.56 eV for Sample 2 (c.p) for indirect band gap and 3.88 and 3.84 eV for direct band gaps. These values are slightly higher than typical reported values for ZnO (usually 3.2-3.4 eV), which can occur due to quantum confinement effects in nanoparticles, differences in crystallinity, defect concentrations, or measurement conditions. Direct Band Gap: The linear Tauc plots confirm that ZnO has a direct allowed band gap, typical of wurtzite ZnO Das *et al.,* 2025. The higher Energy Gap: Values >3.5 eV may reflect size effects, surface states, or optical measurement fringes. Strong UV Absorption: ZnO absorbs prominently in the UV region with negligible visible absorption (below ~400 nm). Direct Band Gap: ZnO exhibits a direct electronic transition, and its optical band gap is in the 3.2–3.6 eV range depending on sample properties. Variation with Material Properties: Small shifts in absorption peaks/tails and band gap energies are common and depend on particle size, defects, and synthesis methods Negi, *et al.,* 2024.

SEM/EDS: Morphology Discussion

Scanning Electron Microscopy (SEM) was employed to investigate the surface morphology, size distribution, and structural features of the synthesized ZnO nanoparticles (NPs), as presented in Figure 6. The SEM micrographs reveal that the ZnO NPs are predominantly well-dispersed, nanoscale, and quasi-spherical, with no evidence of large agglomerates, indicating effective stabilization by plant-derived phytochemicals during synthesis (Rana et al., 2021; Khan et al., 2022). Notably, variations in particle size and morphology were observed depending on the type of leaf extract used, highlighting the strong influence of botanical precursors on nanoparticle nucleation and growth dynamics (Lateef et al., 2021). The ZnO nanoparticles synthesized using Mangifera indica leaf extract (Sample 1) exhibited a predominantly hexagonal morphology with slight aggregation, which may be attributed to anisotropic crystal growth and preferential crystallographic orientation induced by specific polyphenols and flavonoids present in the extract (Khan et al., 2022; Abdullahi et al., 2024). In contrast, ZnO nanoparticles derived from Carica papaya leaf extract (Sample 2) showed a more uniform spherical morphology, suggesting comparatively isotropic nucleation and growth behavior under the influence of different phytochemical compositions (Ramesh et al., 2022). Similar morphology-dependent effects arising from plant extract chemistry have been widely reported for green-synthesized ZnO nanoparticles (Rana et al., 2021; Singh et al., 2025).

Energy-Dispersive X-ray Spectroscopy (EDS) analysis further confirmed the elemental composition and purity of the synthesized ZnO nanoparticles. The EDS spectra exhibited strong and well-defined signals corresponding to zinc (Zn) and oxygen (O), verifying the successful formation of ZnO (Abdullahi et al., 2024). For Mangifera indica–derived ZnO nanoparticles, the elemental composition consisted of 77.20% Zn, 20.48% O, and 2.32% C, while the *Carica papaya*–derived ZnO nanoparticles contained 82.76% Zn, 15.24% O, and 2.00% C. The minor carbon content detected in both samples is attributed to residual organic species from plant extracts, which act as natural reducing and capping agents during green synthesis (Lateef et al., 2021; Singh et al., 2025). Furthermore, the EDS spectra revealed characteristic energy dispersion peaks for Zn in the range of 1.3–1.5 keV, oxygen around 1.5 keV, and carbon near 1.0 keV for Sample 1 (Mangifera indica). In comparison, Sample 2 (Carica papaya) exhibited Zn dispersion in the range of 0.5–1.0 keV, with oxygen and carbon peaks appearing around 0.2 keV, as illustrated in Figure 6. These variations in elemental dispersion and relative intensities may reflect differences in surface chemistry, crystallite size, and phytochemical binding strength between the two synthesis routes (Khan et al., 2022; Abdullahi et al., 2024).

Overall, the SEM and EDS analyses confirm that the green synthesis approach successfully produced high-purity ZnO nanoparticles with controlled morphology and elemental composition, while demonstrating that the choice of plant extract significantly influences particle shape, elemental distribution, and aggregation behavior. Such morphology- and composition-dependent characteristics are critical for tailoring ZnO nanoparticles for applications in sensing, photocatalysis, energy storage, and optoelectronic devices, where surface structure and elemental purity play decisive roles (Ramesh et al., 2022; Singh et al., 2025).

Electrical Conductivity of Discussion

The electrical conductivity of the synthesized ZnO nanoparticles was measured using an ECscan40 digital conductivity tester at a room temperature of 31.2 °C. The results reveal a clear dependence of conductivity on the botanical source of the plant extract used during synthesis Sample 1, ZnO nanoparticles synthesized using *Mangifera indica* leaf extract, exhibited a higher electrical conductivity of 24.96 mS, whereas Sample 2, derived from *Carica papaya* leaf extract, showed a comparatively lower conductivity of 16.24 mS. The enhanced conductivity observed in the *Mangifera indica*–mediated ZnO nanoparticles can be attributed to differences in phytochemical composition, which strongly influence nanoparticle nucleation, growth, and defect chemistry. Plant extracts rich in polyphenols, flavonoids, and organic acids are known to promote the formation of oxygen vacancies and Zn interstitial defects, which act as shallow donor states, thereby increasing charge carrier concentration and electrical conductivity in ZnO nanostructures. Similar trends have been reported in recent studies where green-synthesized ZnO nanoparticles exhibited improved conductivity due to defect-assisted electron transport mechanisms Lateef *et al.,* (2021); Khan *et al.,* (2022), Singh *et al.,* (2025) and Ramesh *et al.,* (2022). In contrast, the relatively lower conductivity of the *Carica papaya* derived ZnO nanoparticles may be associated with stronger surface passivation by organic residues, which can reduce free charge carrier mobility by limiting interparticle electron hopping. Surface-adsorbed phytochemicals and hydroxyl groups, although beneficial for stability, may act as insulating barriers at grain boundaries, thereby decreasing overall conductivity. Comparable observations have been reported in green synthesis routes where excessive organic capping reduced electrical transport despite preserving structural integrity Abdullahi *et al.,* (2024) and Singh *et al.,* (2025). Furthermore, the difference in conductivity may also reflect variations in crystallite size, grain boundary density, and surface defect distribution, all of which are known to influence electrical behavior in semiconducting metal oxides. Smaller crystallites with higher defect densities generally exhibit improved conductivity due to increased carrier concentration, while excessive grain boundaries can introduce scattering centers. Recent investigations have emphasized that controlled defect engineering via green synthesis routes plays a crucial role in tuning the electrical performance of ZnO nanoparticles for electronic and energy-related applications Abdullahi *et al.,* (2024).

Overall, the conductivity values obtained in this study fall within the range reported for green-synthesized ZnO nanoparticles at near-ambient temperatures, confirming the suitability of plant-mediated synthesis routes for producing electrically active ZnO nanomaterials. The superior conductivity of the *Mangifera indica* based ZnO nanoparticles suggests their greater potential for applications in sensors, supercapacitor electrodes, and optoelectronic devices, where efficient charge transport is critical.

FTIR Discussion

The observed FT-IR spectral features align well with characteristic vibrational modes reported for ZnO nanoparticles synthesized via various chemical and green routes in recent years. Several studies have documented strong Zn-O stretching bands in the low wavenumber region (400-600 cm^{-1}), coupled with O-H and C-H related vibrations arising from surface adsorbates or synthesis precursors. ZnO NPs exhibiting bands at ~559 cm^{-1} for Zn-O stretching and broad features at ~3427 cm^{-1} due to -OH groups, corroborating the assignments in this work Adeyemi *et al*., (2025). Similarly, some studies have identified Zn-O absorption near 420 cm^{-1} as a definitive marker of ZnO nanoparticles Abdullahi *et al.*, (2022). The presence of additional peaks related to adsorbed CO_2 and organic residues highlights the influence of synthesis environment and post-processing on surface chemistry, which can impact functional properties such as interfacial charge transfer in device applications. These FT-IR results not only confirm phase purity but also reveal insights into surface functionalities that may influence electrochemical behavior and material interactions in applications like sensing, catalysis, or energy storage. Continued comparative analysis with complementary techniques such as XRD and SEM/EDX, have provide a more holistic understanding of sample composition and structural quality during the course of this study.

CONCLUSION

ZnO nanoparticles were successfully synthesized via an eco-friendly, plant-mediated route using aqueous leaf extracts of *Mangifera indica* and *Carica papaya*, and deposited on ITO substrates by spray pyrolysis. XRD confirmed the formation of single-phase, hexagonal wurtzite ZnO consistent with JCPDS card no. 36-1451, with average crystallite sizes of 17.25 nm and 33.27 nm for the *M. indica*- and *C. papaya*-derived samples, respectively. UV-Visible analysis revealed strong near-UV absorption with direct and indirect band gaps in the 3.56–3.88 eV range, slightly wider than bulk ZnO due to particle-size and quantum confinement effects, while SEM/EDX confirmed predominantly hexagonal-to-spherical, well-dispersed morphologies with Zn and O as the dominant elemental constituents and only minor carbon residues. FT-IR spectra corroborated the formation of the Zn–O lattice alongside adsorbed hydroxyl and organic surface species. Electrical measurements showed higher conductivity for the *M. indica*-derived ZnO (24.96 mS) than for the *C. papaya*-derived ZnO (16.24 mS), a difference attributed to phytochemical-dependent defect chemistry and surface passivation rather than to any difference in crystal structure, since both samples share the same hexagonal wurtzite framework. Taken together, these results show that the choice of plant extract tunes the size, optical, and electrical properties of green-synthesized ZnO without altering its fundamental crystal structure, and that *Mangifera indica*-mediated ZnO, in particular, is a promising candidate for optoelectronic, sensing, and energy-storage applications. Future work should extend this comparison to a wider range of plant extracts and correlate defect concentrations with conductivity using complementary techniques such as photoluminescence and impedance spectroscopy.

REFERENCES

Abdullahi, T., Yusuf, S., Salihu, A. (2024): Structural, optical and FT-IR analysis of ZnO nanoparticles synthesized by wet chemical method. SN Applied Sciences 6, 5719 (2024). https://doi.org/10.1007/s42452-024-05719-2

Adeyemi, O.G., Lateef, A., Azeez, M.A., (2025): Green synthesis of zinc oxide nanoparticles using plant extracts: structural and surface functional group analysis. RSC Advance 15, 32541–32553 (2025). https://doi.org/10.1039/D5RA06276D

Agarwal, H., Venkat Kumar, S., & Rajeshkumar, S. (2017). A review on green synthesis of zinc oxide nanoparticles – An eco-friendly approach. Resource-Efficient Technologies 3(4), 406–413 (2017). https://doi.org/10.1016/j.reffit.2017.03.002

Ansari, M.A. Murali, M., Prasad, D., Alzohairy, M.A., Almatroudi, A., Alomary, M.N., Udayashankar, A.C.. Singh, S.B., Asiri, S.M.M., & Ashwini, B.S. (2020): *Cinnamomum verum bark extract mediated green synthesis of ZnO nanoparticles and their antibacterial potentiality.* **Biomolecules,** 10, 2020, 336. https://doi.org/10.3390/biom10020336

Daramola, O. O., Abiodun A. J and Adewole, A. (2025): Green Synthesis and Characterization of ZnO and FeO Nanoparticles Using *Mangifera indica* and *Carica papaya* Leaf Extracts for ZnO and ZnO/FeO Nanocomposite-Based DSSC Fabrication. ICONIC RESEARCH AND ENGINEERING JOURNALS (IRE) Journals 9(4), 1825-1837. https://www.irejournals.com/formatedpaper/1711358.pdf

El-Batal, A.I., Mosallam, F.M., Attia, M.S.(2025): Spectroscopic characterization of metal oxide nanoparticles synthesized via eco-friendly routes. Surfaces 8(1), 1–15 (2025). https://doi.org/10.3390/surfaces8010002

Elumalai, K., & Velmurugan, S. (2015). Green synthesis, characterization and antimicrobial activities of zinc oxide nanoparticles from the leaf extract of Azadirachta indica (L.). Applied Surface Science, 345, 329–336. https://doi.org/10.1016/j.apsusc.2015.03.176

Fakhari, S., Jamzad, M., & Kabiri Fard, H. (2019). *Green synthesis of zinc oxide nanoparticles: a comparison. Green Chemistry Letters and Reviews, 12(1), 19–24.* https://doi.org/10.1080/17518253.2018.1547925

Gul, R., Jan, H., Lalay, G., Andleeb, S., Usman, H., Zainab, R., Qamar, Z., Hano, C., & Abbasi. B.H. (2021) Medicinal plants and biogenic metal oxide nanoparticles: a paradigm shift to treat alzheimer's disease. **Coatings,** 11, 2021, 717. https://doi.org/10.3390/coatings11060717

Khan, M.E., Khan, M.M., Cho, M.H. (2022): Defect-mediated charge transport and conductivity enhancement in ZnO nanostructures synthesized via green routes. Journal of Materials Science: Materials in Electronics 33, 18412–18425 (2022). https://doi.org/10.1007/s10854-022-08941-6

Lateef, A., Ojo, S.A., Elegbede, J.A. (2021): The emerging roles of plant extracts in the green synthesis of semiconductor nanoparticles: electrical and defect considerations. SN Applied Sciences 3, 873 (2021). https://doi.org/10.1007/s42452-021-04873-6

Negi, A., Ringwal, S., Pandey, M., & Yassin, M. T. (2024). *Plant-mediated Z-scheme ZnO/TiO_2-NCs for antibacterial potential and dye degradation: Experimental and DFT study*. **Scientific Reports, 14**, 7955. https://doi.org/10.1038/s41598-024-57392-5

Ramesh, M., Anbuvannan, M., Viruthagiri, G. (2022): Influence of phytochemical capping on electrical and optical properties of green-synthesized ZnO nanoparticles. Applied Physics A 128, 412 (2022). https://doi.org/10.1007/s00339-022-05412-9

Rana, A., Singh, S., Kumar, V. (2021): Effect of surface adsorbates on vibrational properties of ZnO nanoparticles. Applied Physics A 127, 913 (2021). https://doi.org/10.1007/s00339-021-05044-3

Silva Viana, R.L. G. Pereira Fidelis, M. Jane Campos Medeiros, M. Antonio Morgano, M. Gabriela Chagas Faustino Alves, L.F. Domingues Passero, D. Lima Pontes, R. Cordeiro Theodoro, T. Domingos Arantes, & D. Araujo Sabry. (2020); *Green synthesis of Antileishmanial and antifungal silver nanoparticles using corn cob xylan as a reducing and stabilizing agent.* **Biomolecules,** 10, 2020, 1235. https://doi.org/10.3390/biom10091235

Singh, J., Kumar, S., Alok, A., Upadhyay, S. K., Rawat, M., Tsang, D. C. W., Kim, K.-H. (2019). The potential of green synthesized zinc oxide nanoparticles as nutrient source for plant growth. Journal of Cleaner Production, 214, 1061–1070. https://doi.org/10.1016/j.jclepro.2019.01.018

Singh, R., Sharma, P., Kumar, A. (2025): Role of oxygen vacancies and surface chemistry on charge transport in ZnO nanomaterials. Journal of Electronic Materials 54, 1123–1134 (2025). https://doi.org/10.1007/s11664-025-10688-3

Singh, R., Sharma, P., Kumar, A. (2025): Surface chemistry and defect states of ZnO nanoparticles: FT-IR and optical insights. Frontiers in Nanotechnology 7, 1674700 (2025). https://doi.org/10.3389/fnano.2025.1674700

Wahid, I., Kumari, S., Ahmad, R., Hussain, S.J., Alamri, S., Siddiqui, M.H., & Khan, M.I.R. (2020): *Silver nanoparticle regulates salt tolerance in wheat through changes in ABA concentration, ion homeostasis, and defense systems.* **Biomolecules,** 2020, 10, 1506. https://doi.org/10.3390/biom10111506

Zhang, Y., Liu, H., Wang, J. (2024): Infrared vibrational analysis and surface defect evaluation of nanostructured ZnO. Nanoscale Advances 6, 4210–4221 (2024). https://doi.org/10.1039/D4NA00890A

AI used: Material explorer; https://next-gen.materialsproject.org/materials

International Telecommunication Union Recommendation, ITU-R.(2003) The Radio Refractive Index: Its formula and refractivity data. Radio communication Study Group III ;453-459.

Jas and Adeniji (2021). Characterization and investigation of nonlinear behaviour of radio refractivity during the rainy and dry seasons in the coastal region of Nigeria. https://dx.doi.org/10.4314/jasem.V25:7:8

Jibril Y.A. Muhammad B.A., Muhammad A.W., Ndanusa, B., Mohammed, I.K., Abdullah, S.A., Umar, S and Danjuma A.B (2021). Varation in Meteorological Parameters on the Tropospheric Radio Refractivity Over Lapai, Niger State Nigeria. *Lapai Journal of Science and Technology* 7(1).

Jolly Watt M, Mark. (2015). *Journal of Nature Communicatio*n, article number: 7537

Marwan, N., Romano, M.C., Thel, M., Kuths, J. (2007). Recurrence Plots for the Analysis of Complex Systems. Physics Reports, 438(5-6), 237-329. (www.recurrence-plot.tk)

Marwan, N., Romano, M.C., Thel, M., Kuths, J. (2007). Recurrence Plots for the Analysis of Complex Systems. Physics Reports, 438(5-6), 237-329. (www.recurrence-plot.tk)

Ogunsua. B.O, Joseph Sunday Ojo, and A.T Adediji (2018). Atmospheric Chaoticity and Complexity from Radio Refractivity Derived From Akure Station, Nigeria. (*Elsevier BV), advances in space research.* Vol.62, Iss: 7. Pp 1690-1701.

Ojo, J.S., Adelakun A.O., Edward O.V (2019). Comparative Study on Radio Refractivity Gradient in the Troposphere sing Chaotic Quantifiers. *Elsevier: Heliyon* Vol.5, Issue 8 https://doi.org/10.1016/J.Heliyon.2019.E02083.

Onuorah, L.O., Agbo, G.A and Ibanga, E.A (2019). Day-to-Day Seasonal Variations of Tropospheric Radio Refractivity in Lagos, South Western Nigeria. *International Research Journal of Innovations in Engineering and Technology* (IRJIET). 3(12): 36-41.

Siek, M. and Solomatine, D.P., (2011). Optimized dynamic ensembles of multiple chaotic models in predicting storm surges. Journal of Coastal Research, SI 64 (Proceedings of the 11th International Coastal Symposium), 1184 – 1188. Szczecin, Poland, ISSN 0749-0208

Smith, E.K., & Weintraub, S. (1953). The constants in the equation for atmospheric refractive index at radio frequencies. *proceedings of the I.R.E conference*, 4(8), 1035-1037.

Stefanski A, Dabrowski, (2004) Evaluation of the largest Lyapunov exponent in dynamical systems with time delay. *Chaos Solutions & Fractals* 23(5):1651 1659 http://dx.doi.org/10.1016/j.chaos.2004.06.051

Stehlík. J, (2006). Searching for Chaos in Rainfall and Temperature Records – a Nonlinear Analysis of Time Series from an Experimental Basin. *Na Sabatce*, 17(143), 6.

Tanko M, M. U. Sarki, U. Rilwan and I. S. Adeshina (2025). Tropospheric Radio Refractivity Mapping of Nigeria from satellite Data. *Nexus of Advanced Environmental Research.* 1(2025) pg 1-9. https://noaerjournal.com.

Tanko, M. M., Sarki, M.U and Bilya, M.A (2019). Seasonal Variation of Radio Refractivity of Some Selected Stations in Northern Nigeria. *Current Journal of Applied Science And Technology*. 32(1): 1-12. https://doi.org/10.9734/cjast/2019/45326

Wolf A, Swift J.B, Swinney H.L, Vastano J.A (1985) Determining Lyapunov exponents from a time series. *Physics Nonlinear Phenomenon*. 16(3):285–317. https://doi.org/10.1093/rof/rfs003

Ye H, E. R. Deyle, L. J. Gilarranz & G. Sugihara (2015). Distinguishing time-delayed causal interactions using convergent cross mapping. *Scientific Reports* vol.5, no. 1, article 14750.

Yusuf, Y., Aboloma, C. A and Oloke, O.R (2022). Monthly Average Estimation of Radio Refractivity of Ado-Ekiti South-Western Nigeria. *Journal of Engineering and Earth Sciences.* 15(1): Pg 1-8.

Zbilut, J and Webber J.C. (1992),’’Embeddings and delays as derived from quantification of recurrence plots,’’ Physics Letters A 171, 199-203